Asian Journal of Chemistry; Vol. 38, No. 8 (2026), 2016-2024
ASIAN JOURNAL OF CHEMISTRY
https://doi.org/10.14233/ajchem.2026.36170

Waste to Value-Added-Products: Preparation of Carbon Quantum Dots from Petroleum Coke for the Preparation of Antimicrobial Polyurethane Nanocomposites

N. JEEVA[1], S. RAMKUMAR[2], K. THIRUNAVUKKARASU[1,*] and V. JAISANKAR[2]

[1]Department of Chemistry, Vel Tech Rangarajan Dr. Sagunthala R&D Institute of Science and Technology, Avadi, Chennai-600062, India
[2]PG and Research Department of Chemistry, Presidency College (Autonomous), Chennai-600005, India

*Corresponding author: E-mail: kthirunavukkarasu@gmail.com

Received: 8 April 2026 *Accepted*: 15 June 2026 *Published online*: 7 August 2026 AJC-22427

Carbon quantum dots (CQDs) were prepared using a controlled oxidation process from petroleum coke (petcoke), a low-value by-product, often considered as a waste. Freshly prepared CQDs were then functionalised with vinyltrimethoxysilane (VTMS) to introduce reactive surface silane groups. A silane-functionalised CQD polyurethane (PU) composite (PU/F-CQD) was synthesised using a simple composite synthesis procedure, resulting in uniform dispersion and strong interactions between CQDs and polymer chains. Functionalisation and chemical interactions within the composite were verified by FTIR spectroscopy, whereas XRD analysis confirmed the amorphous nature of the carbon quantum dots (CQDs) and the structural characteristics of the PU matrix. Thermogravimetric analysis established that the composite retained good thermal stability up to 280 ºC. SEM coupled with EDX analysis confirmed the uniform dispersion of CQDs throughout the PU matrix and provided elemental evidence for the composite surface composition. The PU/F-CQD composite exhibited pronounced antifungal activity against pathogenic fungal strains together with substantial *in vitro* anticancer efficacy against the A549 human lung carcinoma cell line. These findings establish a sustainable waste-to-value approach for fabricating multifunctional CQD-polyurethane composites with promising prospects for antifungal and anticancer biomedical applications.

Keywords: Petcoke, Carbon quantum dots, Polyurethane, Vinyltrimethoxysilane, Antifungal activity, Anticancer activity.

INTRODUCTION

Polyurethane (PU) is a versatile polymer widely used in protective coatings [1], biomedical devices [2], filtration membranes [3], foams [4], packaging materials due to its mechanical robustness [5], flexibility and chemical resistance [6]. Long term performance of PU is impaired by microbial colonisation, biofilm development and biodegradation of virgin PU, particularly in medicinal and ecological applications [7,8]. Traditional approaches to impart antimicrobial functionality to PU, including the incorporation of biocides, antibiotics or metal nanoparticles, are frequently associated with limitations such as leaching, cytotoxic effects, microbial resistance and environmental concerns [9]. Carbon-based nanocomposite systems have gained increasing attention as an effective strategy for producing durable, non-leaching and biocompatible antimicrobial PU coatings while preserving their structural and functional stability [10-12].

Carbon quantum dots (CQDs), an important class of carbon based nanoparticles, have attracted considerable research interest owing to their tunable optical properties, excellent biocompatibility, chemical stability, and ability to generate reactive oxygen species (ROS) [13-15]. Their compatibility with polymer matrices makes them attractive nanofillers for the fabrication of functional antimicrobial coatings. CQDs are typically smaller than 10 nm in diameter and possess hybridised sp^2/sp^3 carbon frameworks with surface functionalities including oxygen-, nitrogen- and sulphur-containing groups [14]. These structural features provide high aqueous dispersibility, rich surface chemistry and efficient interactions with microbial cells, making CQDs promising candidates for antimicrobial polymer nanocomposites. Such structural characteristics impart high aqueous dispersibility, strong fluorescence and remarkable surface reactivity. Their antimicrobial activity is primarily attributed to interactions with microbial cell membranes, which induce oxidative stress, disrupt membrane integrity and interfere with essential cellular metabolic processes, leading to broad-spectrum antimicrobial efficacy [15]. Unlike metal-based nanoparticles like Ag or CuO, CQDs have low cytotoxicity, negligible environmental accumula-

This is an open access journal, and articles are distributed under the terms of the Attribution 4.0 International (CC BY 4.0) License. This license lets others distribute, remix, tweak, and build upon your work, even commercially, as long as they credit the author for the original creation. You must give appropriate credit, provide a link to the license, and indicate if changes were made.

tion and improved long-term stability, which makes them an appealing option for biological and environmental applications [16].

Growing interest in sustainable nanotechnology has increased the exploration of waste-derived carbon resources for the synthesis of CQDs. Petroleum coke (petcoke), a carbon rich byproduct generated during the downstream refining of heavy crude oil, is produced in large quantities worldwide. Its low commercial value and disposal challenges create significant environmental concerns [17,18]. The high carbon content and partially graphitic structure of petcoke make it an attractive precursor for carbon nanomaterials. Recent studies have established that petcoke can be converted into CQDs through top-down, hydrothermal and oxidative routes, producing fluorescent nanodots with good stability and abundant surface functional groups suitable for antimicrobial applications [18]. Such conversion transforms an industrial waste into a value-added nanomaterial while supporting resource recovery and circular material utilisation.

CQDs are attractive nanofillers for PU matrices due to their abundant surface functional groups promote strong interfacial interactions with polymer chains, improving compatibility, mechanical integrity and nanoparticle dispersion while minimising aggregation [19]. Their antimicrobial activity originates from multiple complementary mechanisms. Photoactive CQDs generate reactive oxygen species (ROS) under ambient or ultraviolet irradiation, producing oxidative damage to proteins, lipids and nucleic acids, which are essential for microbial survival [16,18]. Surface-functionalised CQDs possess a strong affinity for microbial cell membranes, promoting membrane disruption, leakage of intracellular constituents and eventual cell death [20]. These combined effects make CQD-PU nanocomposites promising alternatives to conventional antimicrobial coatings, which often rely on the release of active agents and suffer from limited durability [21,22].

Although Dubey [23] comprehensively reviewed the conversion of plastic wastes into CQDs, studies involving functionalised CQDs synthesised from industrial waste sources such as petcoke remain scarce. Most reported investigations focus on chemically synthesised CQDs or evaluate CQDs as separate antimicrobial agents rather than as functional reinforcements in polymer matrices [24-26]. The influence of surface functionalised petcoke-derived CQDs on dispersion behaviour, interfacial compatibility, ROS generation and microbial inhibition within PU matrices has not been systematically investigated. Understanding the interplay between composite structure, interfacial chemistry and biological performance is essential for the development of sustainable, high performance antimicrobial materials [27-29].

The present study addresses these knowledge gaps by developing a PU nanocomposite reinforced with vinyltrimethoxysilane (VTMS)-functionalised CQDs synthesised from petcoke. CQDs obtained through a controlled oxidation process offer a scalable waste-to-value approach for converting industrial residues into functional nanomaterials, while PU provides a mechanically robust and biocompatible matrix. Surface functionalisation with VTMS enhances interfacial compatibility by promoting siloxane network formation, leading to improved CQD dispersion, reduced nanoparticle aggregation and stronger CQD-PU interfacial interactions. The structural, optical, thermal, morphological and surface characteristics of the developed nanocomposite are systematically investigated and correlated with its antifungal and anticancer activities. Particular emphasis is placed on understanding the influence of surface functionalisation, interfacial interactions and ROS-mediated mechanisms on the biological performance of the composite.

EXPERIMENTAL

Petroleum coke (Chennai Petroleum Corporation, India), sodium hydroxide, nitric acid, butane-1,4-diol (BDO) (Merck Life Science, India), ethanol, dimethylformamide (DMF) (Avra Chemicals India), sulphuric acid (Thomas Baker, India), vinyltrimethoxysilane (VTMS), hexamethylene diisocyanate (HMDI) and polyethylene glycol (PEG) (Tokyo Chemical Industry, Japan) were employed. Demineralised water was used throughout the work.

Preparation of carbon quantum dots (CQDs): An oxidisation method was used for producing new CQDs from petroleum coke. Initially, petcoke was finely crushed and then added to 45 mL of dil. H_2SO_4. To prevent explosions, 15 mL of dil. HNO_3 was gradually added at specified intervals. The mixture was first sonicated for 2 h, then swirled for 12 h before being neutralised with NaOH [18]. To confirm CQD synthesis, the resulting solution was tested for fluorescence and then the synthesised CQDs were lyophilised to obtain solid CQDs.

Functionalisation of carbon quantum dots (F-CQDs): The as-prepared CQDs were functionalised with VTMS *via* a silanisation reaction. A homogenous suspension was achieved by dispersing 100 mg of CQDs in 50 mL of ethanol and ultrasonicating the mixture for 30 min. Separately, 10 mL of ethanol was used to dissolve 0.5 mL of VTMS and then 1 mL of deionised water was added. The CQD dispersion was then continuously stirred while the hydrolysed VTMS solution was added dropwise. To enhance the condensation between the silanol groups and the CQD surface, the reaction mixture was heated to 60 ºC for 4 h while being continuously stirred [30]. Following the end of the reaction, the liquid was allowed to settle to ambient temperature before being centrifuged for 10 min at 9000 rpm. To get rid of unreacted silane and by-products, the precipitate was repeatedly cleaned with ethanol. The functionalised CQDs (F-CQDs) were then dried into a fine powder and kept in a desiccator for analysis and preparation of composites.

Preparation of F-CQDs-polyurethane composite (PU/F-CQD): An *in situ* polymerisation method was used to incorporate F-CQDs into a PU matrix. In brief, F-CQDs (31.6 mg) was dissolved in 10 mL of DMF and ultrasonicated for 30 min to develop a homogenous suspension. Polyethylene glycol (PEG, 6 g) was transferred to a three-necked round-bottom flask equipped with a mechanical stirrer and a condenser, followed by heating to 60 ºC. The F-CQDs dispersion was introduced dropwise into the PEG under continuous stirring and maintained for 1 h to achieve uniform mixing. Then, HMDI (0.25 mL) was subsequently added dropwise and the reaction mixture was maintained at 60 ºC for 2 h to facilitate prepoly-

mer formation. After completion of the prepolymerisation step, BDO (0.05 mL) was introduced as a chain extender and the reaction was continued for further 1 h until a viscous PU composite homogeneous solution was obtained. The resulting PU/F-CQD composite was cast onto a clean glass substrate and dried at 60 ºC for 24 h to remove residual solvent [31]. The dried composite films were carefully peeled from the substrate and stored in a desiccator until further characterisation. To assess the scalability of the synthesis, laboratory-scale scale-up experiments were performed by proportionally increasing the quantities of all reactants while maintaining identical reaction conditions and processing parameters.

Characterisation of CQDs: The petroleum coke (petcoke) precursor was subjected to proximate analysis using a LOG1-LGICAL SLOC analyser to determine its moisture, volatile matter, ash and fixed carbon contents. The synthesised CQD, F-CQD and PU/F-CQD samples were characterised using complementary analytical techniques. FTIR spectra were recorded over the wavenumber range of 4000-400 cm^{-1} using a BRUKER ALPHA-T ATR-FTIR spectrometer to identify the surface functional groups and chemical interactions. Crystalline characteristics were examined by X-ray diffraction (XRD) using a BRUKER D8 Advance powder X-ray diffractometer equipped with Cu*K*α radiation (λ = 0.1542 nm), with diffraction patterns collected over a 2θ range of 5-100º. Thermal stability and degradation behaviour were evaluated using a Q500 HI-RES thermogravimetric analyser and both thermogravimetric (TGA) and derivative thermogravimetric (DTG) curves were recorded. The surface morphology of the CQD, F-CQD and PU/F-CQD samples was investigated using a high-resolution scanning electron microscope (HR-SEM, Hitachi S2600). The morphology and microstructural features of the synthesised CQDs were further examined by high-resolution transmission electron microscopy (HR-TEM).

Anticancer activity: The anticancer efficiency of F-CQD and PU/F-CQD was evaluated against A549 cell line (a human lung cancer cell line). A549 cell line was obtained from National Centre for Cell Sciences (NCCS), Pune. The cells were maintained in DMEM supplemented with 10% FBS, penicillin (100 U/mL) and streptomycin (100 µg/mL) in a humidified atmosphere of 50 µg/mL CO_2 at 37 ºC. Cells (1×10^5/well) were plated in 24-well plates and incubated in 37 ºC with 5% CO_2 condition. After the cell reaches the confluence, various concentrations of the samples were added and incubated for 24 h. After incubation, the sample was removed from the well and washed with phosphate-buffered saline (pH 7.4) or DMEM without serum. 100 µL/well (5 mg/mL) of 0.5% MTT was added and incubated for 4 h. After incubation, 1 mL of DMSO was added in all the wells. The absorbance at 570 nm was measured with UV-spectrophotometer using DMSO as the blank. Measurements were performed and the concentration required for a 50% inhibition (IC_{50}) was determined graphically. The % cell viability was calculated using the following formula [32,33]:

$$\text{Cell viability (\%)} = \frac{\text{A549 of treated cell}}{\text{A549 of control cells}} \times 100$$

Graphs were plotted using the % of cell viability at *y*-axis and concentration of the sample in *x*-axis. Cell control and sample control were included in each assay to compare the full cell viability assessments.

Antifungal activity: Antifungal activity was determined against *Candida albicans*, *Trichoderma viride* and *Aspergillus niger* by disc diffusion method on Sabouraud Dextrose agar (SDA) medium [34,35]. Sterile SDA medium was poured into Petri plates and allowed to solidify. The fungal inoculum was uniformly spread over the agar surface using a sterile swab pre-moistened with the fungal suspension. Amphotericin B was employed as the positive control. Sterile paper discs loaded with 20 µL of the test samples or the positive control were carefully placed on the inoculated SDA plates. The plates were incubated at 28 ºC for 24 h. Antifungal activity was evaluated by measuring the diameter of the zone of inhibition.

RESULTS AND DISCUSSION

Proximate analysis of petcoke: Proximate analysis is widely employed to evaluate the quality of solid carbonaceous fuels by determining their moisture, volatile matter, ash and fixed carbon contents [36]. Moisture content was determined by heating the sample to approximately 105 ºC until a constant weight was achieved. Low moisture content is desirable since it improves the calorific value and fuel quality. The proximate analysis of petroleum coke revealed a moisture content of 4.8%, volatile matter of 9.17%, ash content of 0.15% and fixed carbon exceeding 80%. The exceptionally high fixed carbon content, together with the low ash and moisture contents, confirms the carbon-rich nature and high purity of the precursor, making it well suited for the synthesis of CQDs. These characteristics support efficient carbonisation, minimize inorganic impurities during processing and contribute to the production of high-quality carbon nanomaterials.

FTIR spectral analysis: The observed bands corresponding to O–H stretching, C=O vibrations and C–O stretching confirm the presence of oxygen-containing functional groups associated with the material surface chemistry. The FTIR spectrum of CQDs, F-CQDs and PU/F-CQDs composite is shown in Fig. 1. The FTIR spectra of pure CQDs show a broad band at 3500-3200 cm^{-1}, which corresponds to O-H stretching vibrations from the surface carboxyl and hydroxyl groups. A peak at 1739 cm^{-1} indicates C=O stretching of carboxylic functionalities, while bands at 1252 and 1039 cm^{-1} correspond to the C-O and C-O-C stretchings, respectively [37]. These oxygen-packed surface groups serve as active silane grafting sites. VTMS functionalisation reduces the broad O-H band, indicating hydroxyl group consumption, while new peaks form at 1103 cm^{-1} (Si-O-Si *str.*) and 612 cm^{-1} (Si-O bend./Si-C vibr./Na-O vibr.), respectively [38]. VTMS covalent attachment to the CQDs surface was confirmed. After the incorporation of F-CQDs into the PU matrix, they produced distinct urethane bands at 2887 cm^{-1} (aliphatic C-H *str.*/vinyl group) and 1339-1235 cm^{-1} (C-N and C-O-C *str.*). The downshifted carbonyl band at 1616 cm^{-1} was caused by hydrogen-bonded urethane carbonyls or contact with CQD sp^2 domains. The composite retained silane-related peaks (1088, 963, 842 and 529 cm^{-1}), showing the structural stability of F-CQDs within the PU network. The development

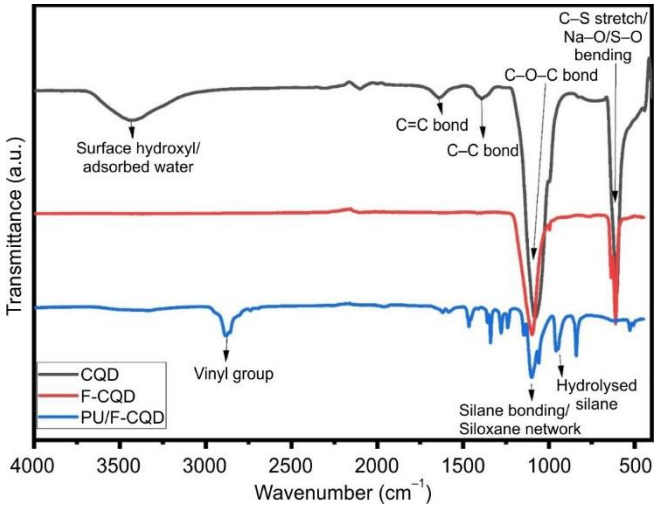

Fig. 1. FTIR spectra of CQDs, F-CQDs and PU/F-CQDs composite

of these FT-IR characteristics from CQDs to F-CQDs and subsequently to the PU composite demonstrated effective surface functionalisation and significant interfacial interactions across the CQDs and PU chains.

XRD analysis: X-ray diffraction was used to investigate the crystalline structure of the synthesised CQDs, F-CQDs and PU composite as shown in Fig. 2. The XRD pattern of the synthesised F-CQDs exhibited a broad diffraction band centred at 2θ = 23-26º, characteristic of partially ordered graphitic (turbostratic) carbon structures commonly reported for CQDs prepared through oxidative routes. The diffuse nature of this reflection reflects a predominantly amorphous carbon framework with only limited graphitic ordering. Distinct diffraction peaks observed between 28º and 33º are unlikely to originate from graphitic carbon, as the characteristic (002) reflection of graphitic domains is appears near 24-26°. These reflections are more likely associated with trace inorganic residues, oxidation-derived byproducts or residual salts remaining after the oxidation, neutralisation and surface functionalisation steps. The diffraction pattern is consistent with nanoscale carbonaceous particles possessing short-range graphitic order embedded within a predominantly disordered carbon matrix [38]. The average crystalline size was calculated using Scherrer's equation:

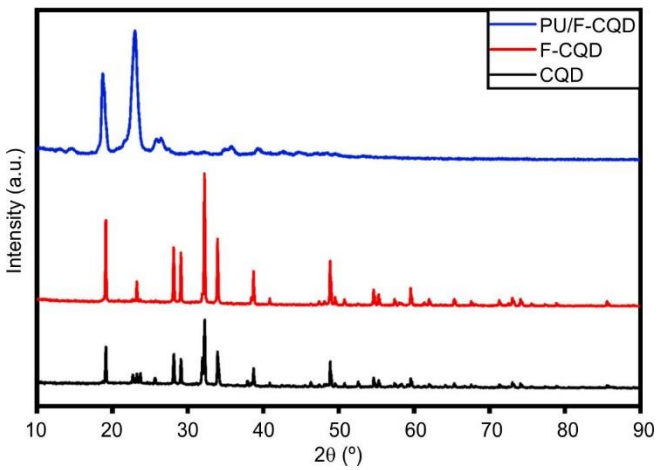

Fig. 2. XRD pattern of CQDs, F-CQDs and PU/F-CQDs composite

$$D = \frac{0.9\lambda}{\beta \cos\theta} \quad (2)$$

The F-CQDs retained the characteristic broad carbon diffraction band, while the sharper reflections became slightly more pronounced after VTMS functionalisation. This behaviour may arise from local structural rearrangement during the silane grafting together with the presence of small amounts of residual inorganic species associated with the surface modification process. The XRD pattern of the PU/F-CQD composite was dominated by two broad diffraction peaks centred at approximately 18.75º and 23º, corresponding to the semicrystalline hard and soft segments of the polyurethane matrix. No distinct diffraction features attributable to F-CQDs were detected, implying that the nanodots remained well dispersed within the polymer matrix without forming detectable crystalline aggregates. The absence of additional crystalline reflections supports strong interfacial compatibility between the functionalised CQDs and polyurethane, preserving the semi-crystalline nature of the polymer while preventing long-range ordering of the dispersed nanofiller.

TGA-DTG analysis: The thermal stability and decomposition behaviour of the PU/F-CQDs composite were evaluated with thermogravimetric analysis (TGA) and its derivative thermogravimetric (DTG) curve. The TGA curve (Fig. 3) shows a weight loss profile in two stages, which is typical of PU-based nanocomposites. At 280-330 ºC, the PU soft segments thermally degraded, resulting in a weight loss of approximately 77.66% including the breakage of urethane linkages, the disintegration of polyol chains and the gradual degradation of functional groups on the surface of F-CQDs. The corresponding DTG peak within this temperature range marks the maximum decomposition rate, where degradation of the PU matrix accounts for the largest fraction of mass loss. A second weight-loss stage of approximately 20.54% occurs between 400 and 430 ºC and is attributed to the decomposition of the PU hard segments together with thermally stable carbonaceous residues formed during the initial degradation process. The DTG maximum in this region is associated with the breakdown of these relatively stable region.

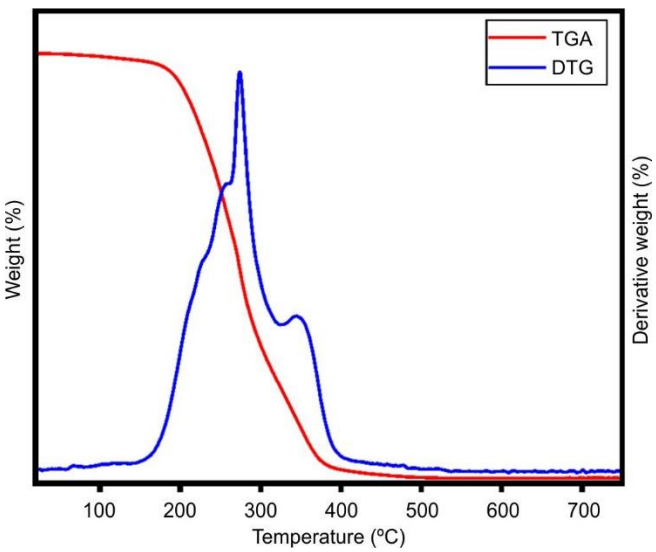

Fig. 3. TGA and DTG curve of PU/F-CQDs composite

The incorporation of F-CQDs alters the thermal degradation behaviour of the PU matrix, resulting in a characteristic multistep decomposition pattern and delaying the onset of thermal decomposition. This effect arises from strong interfacial interactions between the surface functional groups of the CQDs and the PU chains, which restrict polymer chain mobility and enhance resistance to thermal degradation. Comparable thermal stabilisation has been reported for CQD- and other carbon-based polymer nanocomposites [39,40]. The TGA-DTG results demonstrate thermal stability of the PU/F-CQD composite up to approximately 280 ºC, together with a well-defined degradation profile, making the material suitable for biomedical applications.

SEM analysis: Fig. 4a-f presents the SEM micrographs of CQDs, F-CQDs and the PU/F-CQDs composite. The pristine CQDs consist of nanoscale particles with a predominantly quasi-spherical morphology. Their extremely small particle size and high surface energy promote particle agglomeration, a characteristic commonly observed in CQDs synthesised through top-down oxidative routes. The F-CQDs retain a nearly spherical morphology, although the degree of aggregation becomes more pronounced. This behaviour can be attributed to strong inter-particle interactions arising from the oxygen-containing functional groups introduced during oxidation and the silane moieties grafted during VTMS functionalisation [41].

The PU/F-CQDs composite exhibits a dense, homogeneous and continuous polymer matrix with the F-CQDs well distributed throughout the PU network. No visible voids, cracks or phase-separated regions are observed, reflecting good compatibility between the F-CQDs and the PU matrix. The improved dispersion is attributed to the surface functional groups of the F-CQDs, which promote strong chemical and physical interactions with the urethane segments of polyurethane, resulting in enhanced interfacial adhesion and effective incorporation of the nanofiller within the polymer matrix [42].

SEM-EDX analysis: SEM-EDX analysis of the samples clearly revealed the surface atomic composition after functionalisation and subsequent incorporation into the PU matrix (Fig. 5). The surface composition of CQDs showed dominance of O, Na and S atoms. Residual sodium detected on the CQD surface originated from the neutralisation step, nitrogen atoms introduced by dilute HNO_3 were completely removed during synthesis, while sulphur contents were retained because petcoke was used as the precursor.

Following VTMS functionalisation, the surface carbon content increased due to grafting of silane onto the CQDs. The disappearance of surface hydroxyl groups was consistent with the FTIR analysis, while the participation of oxygen-containing groups in the silanisation reaction accounted for the relatively preserved oxygen content. Surface sodium concentration decreased markedly after functionalisation, with the Na atomic percentage decreases from 27.20% to 18.98%, reflecting the effective removal of residual sodium species during the modification process.

Silicon was detected in the F-CQDs after VTMS functionalisation, with a surface atomic concentration of 0.40%. The relatively low silicon signal is attributed to the limited surface exposure of silane moieties and the lower sensitivity of SEM-EDX toward light elements present in small quantities. EDX analysis confirmed carbon and oxygen as the dominant elements, accompanied by a minor silicon contribution arising from VTMS grafting. Although nitric acid was employed during the oxidation process, no detectable nitrogen peak was observed in the final spectrum, reflecting the effective removal of nitrogen-containing residual species during purification and neutralisation. This observation suggests that

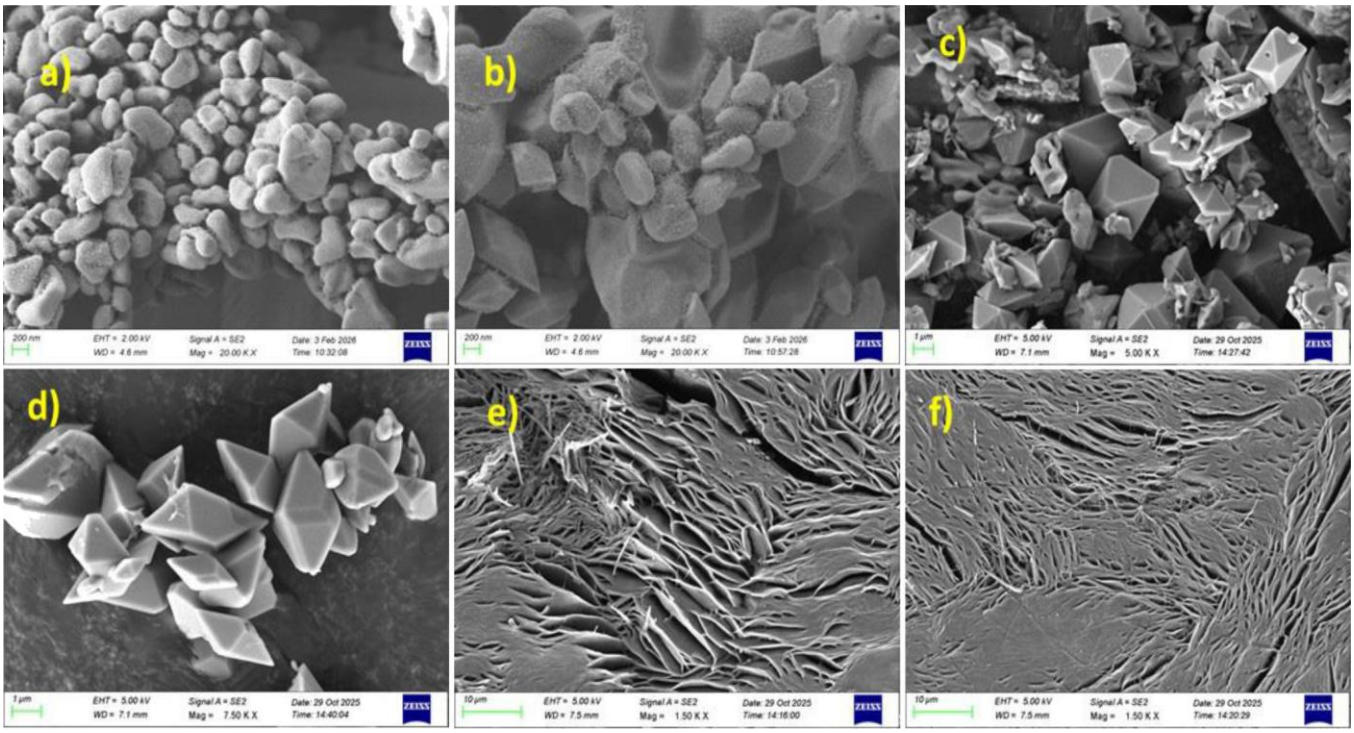

Fig. 4. SEM images of (a,b) CQDs, (c,d) F-CQDs and (e,f) F-CQDs/PU

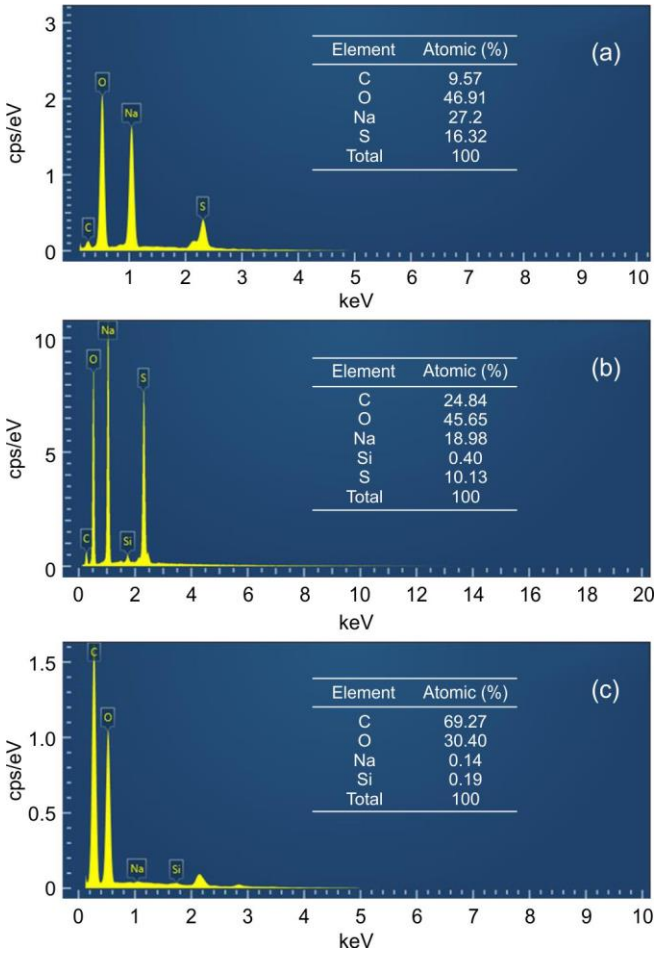

Fig. 5. SEM-EDX results of (a) CQDs, (b) F-CQDs and (c) PU/F-CQDs

nitric acid primarily served as an oxidizing agent rather than a nitrogen-doping precursor during CQDs synthesis. In the PU/F-CQDs nanocomposite, the PU matrix contributed to a higher surface carbon content, while the relative concentrations of oxygen, sodium and silicon decreased following encapsulation of the F-CQDs within the polymer network.

TEM analysis: The morphology and microstructural characteristics of the synthesised CQDs were examined by TEM. The CQDs (Fig. 6a) possess a predominantly quasi-spherical morphology with particle sizes below 10 nm and a relatively uniform size distribution. Slight particle agglomeration is observed, which can be attributed to the high surface energy of the CQDs together with the abundance of surface functional groups generated during oxidative synthesis and partial aggregation during sample drying [43].

The SAED pattern (Fig. 6b) consists of diffuse concentric diffraction rings rather than discrete spots, characteristic of a predominantly amorphous carbon matrix containing embedded nanocrystalline graphitic domains [13]. This microstructure is consistent with the broad diffraction features observed in the XRD analysis and reflects the coexistence of short-range graphitic ordering within an amorphous carbon framework. The combined TEM and SAED observations establish the successful synthesis of nanoscale CQDs with quasi-spherical morphology, partial graphitic ordering and structural characteristics suitable for incorporation into polymer nanocomposites.

On the basis of the above characterisation studies, a schematic diagram was drawn for the synthesis of PU nanocomposite of F-CQDs (Fig. 7).

***In vitro* anticancer activity:** An *in vitro* cell viability assay was performed to evaluate the anticancer activity of F-CQDs and the PU/F-CQDs composite against human lung carcinoma (A549) cells. As presented in Table-1, F-CQDs reduced cell viability in a concentration-dependent manner. This response is attributed to their nanoscale dimensions and abundant surface functional groups, which facilitate cellular

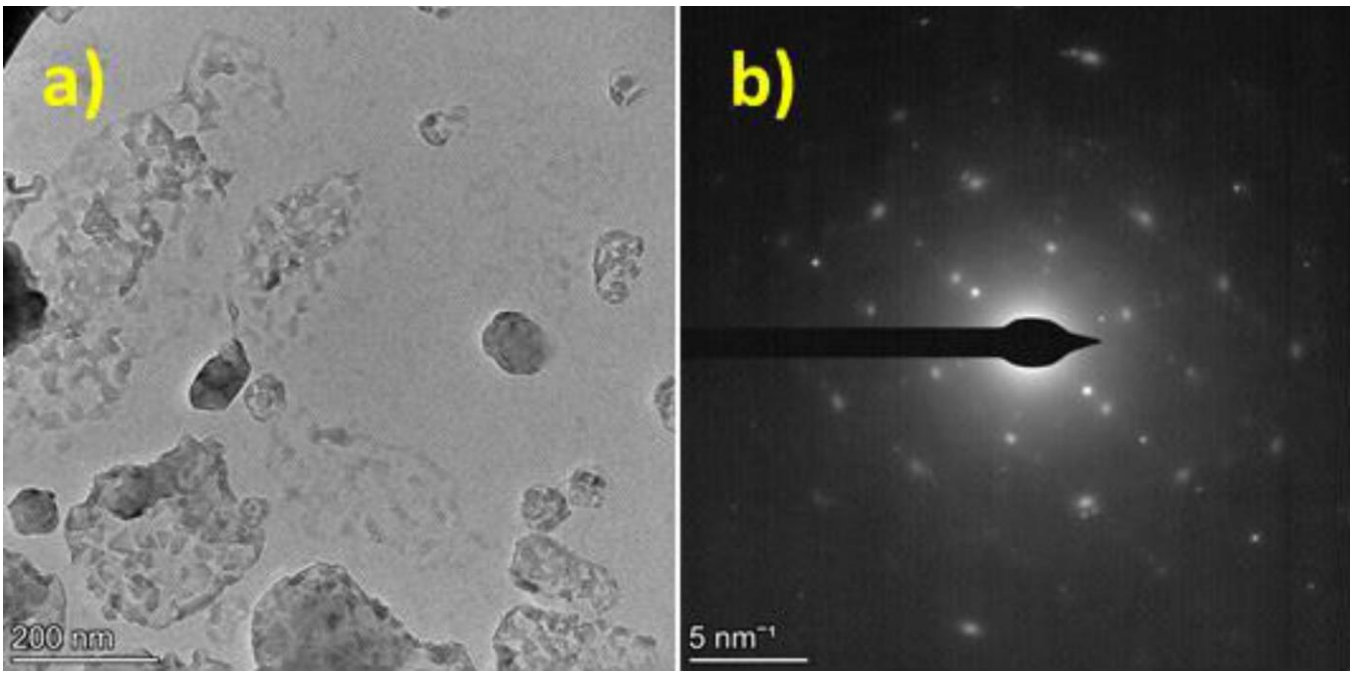

Fig. 6. (a) TEM image and (b) SAED patterns of CQDs

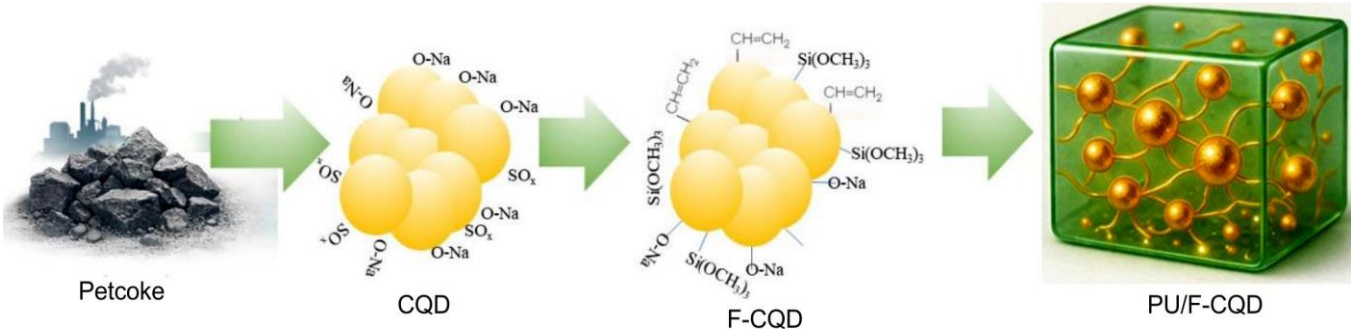

Fig. 7. Synthesis of PU nanocomposite (not drawn to scale)

TABLE-1
ANTICANCER ACTIVITY OF F-CQDs ON A549 CELLS

Concentration (µg/mL)	F-CQD on A549 cells		PU/F-CQD on A549 cells	
	Absorbance (O.D)	Cell viability (%)	Absorbance (O.D)	Cell viability (%)
1000	0.138	18.87	0.173	23.66
500	0.181	24.76	0.221	30.23
250	0.226	30.91	0.269	36.79
125	0.270	36.93	0.317	43.36
62.5	0.315	43.09	0.364	49.79
31.2	0.358	48.97	0.411	56.22
15.6	0.403	55.12	0.458	62.65
7.8	0.446	61.01	0.506	69.22
Cell control	0.731	100	0.731	100

uptake and promote intracellular ROS generation, leading to oxidative stress and cell death [41].

At equivalent concentrations, the PU/F-CQDs composite maintained higher cell viability than the F-CQDs alone (Fig. 8). This behaviour is attributed to the immobilisation and uniform dispersion of the F-CQDs within the PU matrix, which limits direct nanoparticle–cell interactions and moderates non-specific cytotoxic effects. The PU matrix serves as a biocompatible support, regulating the accessibility of the embedded CQDs while preserving their structural stability [44]. Although the PU/F-CQDs composite exhibited lower cytotoxicity than the free F-CQDs, its improved stability and sustained presentation of the functionalised CQDs make it a promising platform for controlled anticancer drug delivery and other biomedical applications.

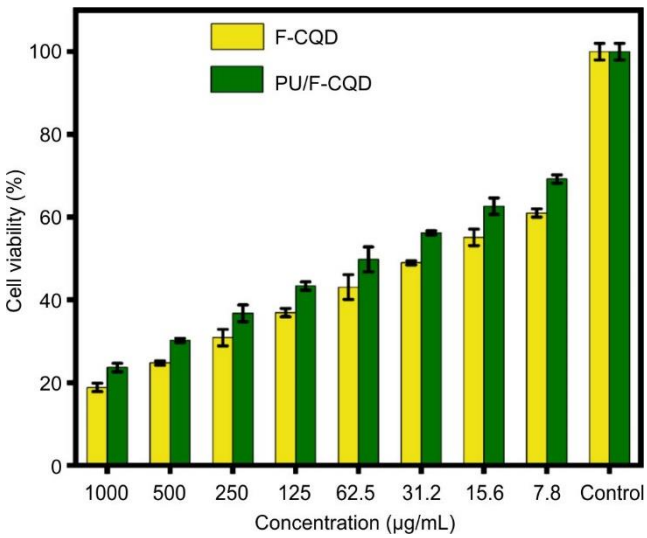

Fig. 8. Comparative cell viability of F-CQDs and PU/F-CQDs

Antifungal activity: The antifungal activities of F-CQDs and the PU/F-CQD composite were evaluated against *C. albicans*, *T. viride* and *A. niger* using the agar diffusion method (Table-2). F-CQDs exhibit distinct zones of inhibition against all tested fungal strains, reflecting their inherent antifungal activity. This behaviour can be attributed to their nanoscale dimensions, high surface reactivity and abundant oxygen-containing functional groups, which promote interactions with fungal cell membranes and compromise membrane integrity [45].

The PU/F-CQDs composite exhibited appreciable antifungal activity, confirming that the incorporation of F-CQDs effectively imparts antifungal functionality to the PU matrix. The uniform distribution of the F-CQDs within the polymer network facilitates effective contact between the active nanofiller and fungal cells while maintaining the structural integrity of the composite. The antifungal and anticancer responses observed for the F-CQDs and PU/F-CQDs composite are likely influenced by their surface chemistry, nanoscale size and interactions with biological membranes. Although ROS generation has been proposed as a plausible mechanism for the biological activity of carbon-based nanomaterials, no direct ROS measurements were performed in the present study. A comparison of the antifungal performance of the developed PU/F-CQDs composite with previously reported polymer- and polyurethane-based nanocomposites is presented in Table-3.

Conclusion

In this study, conversion of petroleum coke into functional CQDs provides a sustainable waste-to-value route using simple

TABLE-2
ANTIFUNGAL ACTIVITIES OF F-CQDs AND PU/F-CQDs

Organisms	Zone of inhibition (mm)							
	F-CQD				PU/F-CQD			
	1000 µg/mL	750 µg/mL	500 µg/mL	Standard	1000 µg/mL	750 µg/mL	500 µg/mL	Standard
Candida albicans	13	10	9	26	14	10	9	30
Trichoderma viride	10	9	9	18	10	9	9	13
Aspergillus niger	11	10	9	16	15	15	13	18

TABLE-3
NANOCOMPOSITES AND THEIR ANTIFUNGAL ACTIVITIES: COMPARISON TABLE FROM THE LITERATURE

Nanocomposite system	Key role	Fungus studied	Test method	Limitations	Ref.
Chitosan/graphene oxide	Synergetic effect of chitosan & graphene oxide	*A. niger*, *T. viride* and *C. albicans*	Disc diffusion	Active for *A. niger* and *T. viride* (multicellular); but not active for *C. albicans* (unicellular)	[36]
COIHPU2@GO2	Amphiphilic nature of the hybrid matrix and the presence of GO nanosheets	*C. albicans* and *A. niger*	Disc diffusion	Moderate activity	[46]
pMWCNT-CD polyurethane & pMWCNT-CD/Ag-TiO_2 polyurethane	Possible reactive oxygen species formation	*A. ochraceus* and *A. fumigatus*	Disc diffusion	pMWCNT-CD/Ag-TiO_2 shows greater activity	[47]
CAgPU@PNM	Uniformly dispersed Ag nanostructures within the polymer matrix	*C. albicans*	Disc diffusion	Multicellular fungi not tested	[48]
F-CQD/PU	VTMS-functionalised CQDs	*A. niger*, *T. viride* and *C. albicans*	Disc diffusion	Needs further study for understanding the mechanism	This work

and scalable processing. CQDs were successfully synthesised from low-cost petroleum coke and subsequently functionalised with vinyltrimethoxysilane (VTMS) to improve their compatibility with a PU matrix. The resultant PU/F-CQDs composite was systematically characterised, which confirmed the formation of nanosize CQDs, successful surface functionalisation, uniform dispersion within the polymer network and enhanced thermal stability of the composite system. The biological assessment established that the PU/F-CQDs composite possesses sustained antifungal and anticancer activity, attributed to improved dispersion, stability and interfacial compatibility of the F-CQDs within the PU matrix.

ACKNOWLEDGEMENTS

One of the authors, N. Jeeva thanks Research Studies department Vel Tech Rangarajan Dr. Sagunthala R&D Institute of Science and Technology, Avadi, Chennai, India for their continuous support for her thesis work.

CONFLICT OF INTEREST

The authors declare that there is no conflict of interests regarding the publication of this article.

DECLARATION OF AI-ASSISTED TECHNOLOGIES

During the preparation of this manuscript, the authors used an AI-assisted tool(s) to improve the language and no data, results or scientific conclusions were generated by AI. All analyses, interpretations and conclusions are the authors' own. The authors reviewed and edited the content and take full responsibility for the published work.

REFERENCES

1. Y. Zhou, M. Zhang, H. Hu, C. Bi, H. Zhang, Y. Ye and C. Yan, *J. Polym. Sci.*, **64**, 197 (2026); https://doi.org/10.1002/pol.20250479
2. N.H. Khan, M.S. Mohamed Ali and M.N. Hasan, *Eur. Polym. J.*, **243**, 114460 (2026); https://doi.org/10.1016/j.eurpolymj.2025.114460
3. G.G. Njema, S.N. Lemomo, P.K. Tanui and J.K. Kibet, *Nat. Sci.*, **6**, e70041 (2026); https://doi.org/10.1002/ntls.70041
4. P.A. Silveira da Silva, T.L.N. Acosta, L.Q. Minillo, R.A. Delucis, P.H.G. Cademartori and A.P. Acosta, *Mater. Res. Bull.*, **197**, 113968 (2026); https://doi.org/10.1016/j.materresbull.2025.113968
5. M. Bilal, M. Arslan, S. Khan, J. Shi, Z. Li, Y. Guo, X. Sun and Z. Xiaobo, *Trends Food Sci. Technol.*, **166**, 105400 (2025); https://doi.org/10.1016/j.tifs.2025.105400
6. X. Zhu, Z. Yan, X. Zou, N. Yu, G.H. Hu, S. Zhang, J. Du, S. Zhang, W. Wu and H. Zhao, *J. Mater. Chem. C Mater. Opt. Electron. Devices*, **14**, 1747 (2026); https://doi.org/10.1039/D5TC03366G
7. P. Sikdar, T.M. Dip, A.K. Dhar, M. Bhattacharjee, M.S. Hoque and S.B. Ali, *J. Appl. Polym. Sci.*, **139**, e52832 (2022); https://doi.org/10.1002/app.52832
8. C.O. Adetunji, O.T. Olaniyan, O.A. Anani, A. Inobeme and J.T. Mathew, *ACS Symp. Ser.*, **1380**, 393 (2021); https://doi.org/10.1021/bk-2021-1380.ch014
9. S. Farah, D.G. Anderson and R. Langer, *Adv. Drug Deliv. Rev.*, **107**, 367 (2016); https://doi.org/10.1016/j.addr.2016.06.012
10. A. Ali, M.Z. Khan, S. Rasheed and R. Imtiaz, *Micro*, **6**, 5 (2026); https://doi.org/10.3390/micro6010005
11. P. Maurya, A. Majumdar, B.S. Butola, P. Goswami and R. Bhattacharyya, *J. Text. Inst.*, **117,** 686 (2026); https://doi.org/10.1080/00405000.2025.2518342

12. Y. Ahmadi, N. Moeini, M. Yadav and S. Ahmad, in eds. C.M. Hussain, Antimicrobial Polymer Nanocomposite Films and Coatings, In: Handbook of Polymer Nanocomposites for Industrial Applications, Elsevier, Chap. 12, pp. 379-379 (2021); https://doi.org/10.1016/B978-0-12-821497-8.00012-5
13. S.N. Baker and G.A. Baker, *Angew. Chem. Int. Ed.*, **49**, 6726 (2010); https://doi.org/10.1002/anie.200906623
14. S.Y. Lim, W. Shen and Z. Gao, *Chem. Soc. Rev.*, **44**, 362 (2015); https://doi.org/10.1039/C4CS00269E
15. K. Hola, Y. Zhang, Y. Wang, E.P. Giannelis, R. Zboril and A.L. Rogach, *Nano Today*, **9**, 590 (2014); https://doi.org/10.1016/j.nantod.2014.09.004
16. Ł. Janus, M. Piątkowski, J. Radwan-Pragłowska, D. Bogdał and D. Matysek, *Nanomaterials*, **9**, 274 (2019); https://doi.org/10.3390/nano9020274
17. M. Wu, Y. Wang, W. Wu, C. Hu, X. Wang, J. Zheng, Z. Li, B. Jiang and J. Qiu, *Carbon*, **78**, 480 (2014); https://doi.org/10.1016/j.carbon.2014.07.029
18. R.L.B. Cabral, E.R.V.P. Galvão, P.B.A. Fechine, F.M.F. Galvão and J.H.O. Nascimento, *RSC Adv.*, **14**, 19953 (2024); https://doi.org/10.1039/D4RA01196A
19. A. Navidfar, M.I. Peker, E. Budak, C. Unlu and L. Trabzon, *Compos., Part B Eng.*, **247**, 110310 (2022); https://doi.org/10.1016/j.compositesb.2022.110310
20. H. Thi Thu, L.T. Anh, D.T. Huong and D.N. Huyen, *Mater. Adv.*, **7**, 2268 (2026); https://doi.org/10.1039/D5MA00802F
21. L. Dall Agnol, F.T.G. Dias and O. Bianchi, *Prog. Org. Coat.*, **179**, 107492 (2023); https://doi.org/10.1016/j.porgcoat.2023.107492
22. M. Kováčová, Z.M. Marković, P. Humpolíček, H. Švajdlenková, M. Mičušík, A. Kleinová, M. Danko, P. Kubát, J. Vajďák, Z. Capáková, M. Lehocký, L. Münster, B.M. Todorović Marković and Z. Špitalský, *ACS Biomater. Sci. Eng.*, **4**, 3983 (2018); https://doi.org/10.1021/acsbiomaterials.8b00582
23. P. Dubey, *Waste Biomass Valoriz.*, **16**, 6373 (2025); https://doi.org/10.1007/s12649-025-03118-1
24. S.S. Hindi, J.S.M. Sabir, U.M. Dawoud, I.M. Ismail, K.A. Asiry, Z.M. Mirdad, K.A. Abo-Elyousr, M.H. Shiboob, M.O.I. Albureikan, M.A. Gabal, R.A. Alanazi and O.H.M. Ibrahim, *Polymers*, **15**, 2660 (2023); https://doi.org/10.3390/polym15122660
25. L.H. Slewa, B.A. Gozeh, D.S. Ismael, N.Q. FaqeAbdulla and H.O. Othman, *Bionanoscience*, **14**, 2705 (2024); https://doi.org/10.1007/s12668-024-01486-x
26. Y. Wu, C. Li, H.C. van der Mei, H.J. Busscher and Y. Ren, *Antibiotics*, **10**, 623 (2021); https://doi.org/10.3390/antibiotics10060623
27. M. Kováčová, Z.M. Marković, P. Humpolíček, H. Švajdlenková, M. Mičušík, A. Kleinová, M. Danko, P. Kubát, J. Vajďák, Z. Capáková, M. Lehocký, L. Münster, B. M. Todorović Marković and Z. Špitalský, *ACS Biomater. Sci. Eng.*, **4**, 3983 (2018); https://doi.org/10.1021/acsbiomaterials.8b00582
28. B.P. Chang, A. Gupta, R. Muthuraj and T.H. Mekonnen, *Green Chem.*, **23**, 5337 (2021); https://doi.org/10.1039/D1GC01115D
29. S. Simões, *Materials*, **17**, 5997 (2024); https://doi.org/10.3390/ma17235997
30. G. Hu, H. Xu, Z. Wang, G. Xie, Y. Lv, Y. He, H. Zhang, X. Zhang and B. Lei, *Mater. Res. Bull.*, **173**, 112698 (2024); https://doi.org/10.1016/j.materresbull.2024.112698
31. X. Liu, Z. Ge, W. Zhang and Y. Luo, *High Perform. Polym.*, **32**, 611 (2020); https://doi.org/10.1177/0954008319891758
32. O. Sen, S. Jana, G. Nandi and S. Manna, *Int. J. Polym. Mater.*, **74**, 555 (2024); https://doi.org/10.1080/00914037.2024.2344618
33. G.M. Hemalatha, K. Thirunavukkarasu and C.R. Kumar, *Int. J. Appl. Pharm.*, **14**, 168 (2022); https://doi.org/10.22159/ijap.2022.v14ti.48.
34. W.F. Khalil, G.S. El-Sayyad, W.M.A. El Rouby, M.A. Sadek, A.A. Farghali and A.I. El-Batal, *Int. J. Biol. Macromol.*, **164**, 1370 (2020); https://doi.org/10.1016/j.ijbiomac.2020.07.205
35. G.M. Hemalatha, K. Thirunavukkarasu, C.R. Kumar, M. Thamim and K. Thirumoorthy, *ChemistrySelect*, **8**, e202204898 (2023); https://doi.org/10.1002/slct.202204898.
36. S. Renukadevi, V. Manimozhi, E.K.T. Sivakumar and V. Jaisankar, *J. Indian Chem. Soc.*, **102**, 101760 (2025); https://doi.org/10.1016/j.jics.2025.101760
37. R. Friedel and G. Carlson, *Fuel*, **51**, 194 (1972); https://doi.org/10.1016/0016-2361(72)90079-8
38. Y.P. Sun, B. Zhou, Y. Lin, W. Wang, K.A.S. Fernando, P. Pathak, M.J. Meziani, B.A. Harruff, X. Wang, H. Wang, P.G. Luo, H. Yang, M.E. Kose, B. Chen, L.M. Veca and S.-Y. Xie, *J. Am. Chem. Soc.*, **128**, 7756 (2006); https://doi.org/10.1021/ja062677d
39. Y. Zhang, S. Xu, J. Liu, K. Zhang, Y. Guan and S. Li, *Appl. Surf. Sci.*, **655**, 159645 (2024); https://doi.org/10.1016/j.apsusc.2024.159645
40. J. Pagacz, E. Hebda, B. Janowski, D. Sternik, M. Jancia and K. Pielichowski, *Polym. Degrad. Stab.*, **149**, 129 (2018); https://doi.org/10.1016/j.polymdegradstab.2018.01.028
41. Y. Wang and A. Hu, *J. Mater. Chem. C Mater. Opt. Electron. Devices*, **2**, 6921 (2014); https://doi.org/10.1039/C4TC00988F
42. T.K. Gupta, B.P. Singh, S. Teotia, V. Katyal, S.R. Dhakate and R.B. Mathur, *J. Polym. Res.*, **20**, 169 (2013); https://doi.org/10.1007/s10965-013-0169-6
43. T. Garcia-Millán, J. Ramos-Soriano, M. Ghirardello, X. Liu, C.M. Santi, J.-C. Eloi, N. Pridmore, R.L. Harniman, D.J. Morgan, S. Hughes, S.A. Davis, T.A.A. Oliver, K.M. Kurian and M.C. Galan, *ACS Appl. Mater. Interfaces*, **15**, 44711 (2023); https://doi.org/10.1021/acsami.3c08200
44. S.M. Mousavi, S.A. Hashemi, M.Y. Kalashgrani, N. Omidifar, S. Bahrani, N. Vijayakameswara Rao, A. Babapoor, A. Gholami and W.-H. Chiang, *Polymers*, **14**, 617 (2022); https://doi.org/10.3390/polym14030617
45. E.A. Diab, M. Ghali and M.M. Mosaad, *Sci. Rep.*, **15**, 16199 (2025); https://doi.org/10.1038/s41598-025-99841-9
46. M. Alam, N.M. Alandis, A. Ahmad, M. Ahmed and P. Karuppiah, *Polym. Compos.*, **47**, 9537 (2026); https://doi.org/10.1002/pc.70776
47. A.L. Taka, B.P. Doyle, E. Carleschi, T.Y. Fonkui, R. Erasmus, E. Fosso-Kankeu, K. Pillay and X.Y. Mbianda, *Mater. Sci. Eng. C*, **115**, 111092 (2020); https://doi.org/10.1016/j.msec.2020.111092
48. Shaily, F. Zafar, A. Ghosal, M. Alam, H. Naaz, T. Fatma and N. Nishat, *J. Mol. Struct.*, **1348**, 143333 (2025); https://doi.org/10.1016/j.molstruc.2025.143333